 doi:10.20944/preprints202108.0520.v1

Distinct exosomal miRNA profiles from BALF and lung tissue from COPD and IPF patients

Gagandeep Kaur[1], Krishna P Maremanda[1], Michael Campos[2], Hitendra S Chand[3], Feng Li[4], Nikhil Hirani[4], M.A. Haseeb[5] and Irfan Rahman[1*]

[1]Department of Environmental Medicine, University of Rochester Medical Center, Rochester, NY, USA

[2] Division of Pulmonary, Allergy, Critical Care, University of Miami School of Medicine Miami, FL, USA

[3] Department of Immunology and Nanomedicine, Florida International University, Miami, FL, USA

[4] Centre for Inflammation Research, Queen's Medical Research Institute, University of Edinburgh, Edinburgh, EH16 4TJ, UK

[5] Department of Cell Biology, SUNY Downstate Health Sciences University, Brooklyn, New York, USA

*Correspondence should be addressed to:
Irfan Rahman, Ph.D.
Department of Environmental Medicine
University of Rochester Medical Center
Box 850, 601 Elmwood Avenue
Rochester 14642, NY, USA
Tel: 1 585 275 6911
E-mail: irfan_rahman@urmc.rochester.edu

Short running title: Exosomal miRNA signature in COPD and IPF

Preprints (www.preprints.org) | NOT PEER-REVIEWED | Posted: 27 August 2021 doi:10.20944/preprints202108.0520.v1

Abstract

Background: Chronic Obstructive Pulmonary Disease (COPD) and Idiopathic Pulmonary Fibrosis (IPF) are chronic, progressive lung ailments which are characterized by distinct pathologies. Early detection biomarkers and disease mechanisms for these debilitating diseases are lacking. Exosomes are small extracellular vesicles attributed to carry proteins, mRNA, miRNA and sncRNA to facilitate cell-to-cell communication under normal and diseased conditions. Exosomal miRNAs have been studied in relation to many diseases. However, there is little to no knowledge regarding the miRNA population of BALF or the lung tissue derived exosomes in COPD and IPF. Here, we determined and compared the miRNA profiles of BALF and lung tissue-derived exosomes from healthy non-smokers, healthy smokers, and patients with COPD and IPF in independent cohorts. **Results:** Exosome characterization using NanoSight particle tracking and TEM demonstrated that the BALF-derived exosomes were approximately 89.85 nm in size and ~2.95 X 10^{10} particles/mL. Lung-derived exosomes were ~146.04 nm in size and ~2.38 X 10^{11} particles/mL. NGS results identified three differentially expressed miRNAs in the BALF, while one in the lung-derived exosomes from COPD patients as compared to healthy non-smokers. Of these, three- and five-fold downregulation of miR-122-5p amongst the lung tissue-derived exosomes from COPD patients as compared to healthy non-smokers and smokers, respectively. Interestingly, there were key 55 differentially expressed miRNAs in the lung tissue-derived exosomes of IPF patients compared to non-smoking controls. **Conclusions:** Overall, we identified specific miRNAs to develop as biomarkers or targets for pathogenesis of these chronic lung diseases.

Keywords: Exosomes, miRNA, COPD, Biomarker, BALF and Lung tissue.

 doi:10.20944/preprints202108.0520.v1

Introduction

Tobacco smoking remains the most prevalent preventable cause of morbidity and mortality, worldwide. Comprising of more than 5000 compounds (1), cigarette smoke is the leading risk-factor for developing chronic obstructive pulmonary disease (COPD) and idiopathic pulmonary fibrosis (IPF) in humans. Despite their distinct clinical features, both COPD and IPF can be defined as chronic, progressive airway diseases associated with increased risk of cancer development (2, 3). The current therapies for these conditions are mainly palliative; and the chief reason of this is due to limited understanding of the pathophysiology of these respective ailments (4, 5).

Evidence from literature suggest the role of extracellular vesicles/exosomes in the disease severity and outcome in COPD and IPF (6-10). Exosomes function to maintain homeostasis and intracellular stability. However, they also become pathosomes due to harmful stimulus (e.g. tobacco smoke) and can participate in the progression of diseases. In this respect, exosomes are known to cause pathological changes including oxidative stress, chronic inflammation, apoptosis, aging, epigenetic alterations and multi-organ dysfunction in COPD (11-14). Interestingly, exosomes are produced and released in the sputum, serum and BALF of COPD patients in large quantities which makes them a useful target to develop non-invasive diagnostics in COPD. Previous studies have mostly compared the serum-derived exosome populations from COPD patients and healthy individuals (15-20). Similarly, exosomes isolated from the biological fluids cause pro-inflammatory responses in lung cells (11, 21, 22). However, there is little to no knowledge about the BALF or the lung tissue-derived exosome populations in COPD or IPF.

Preprints (www.preprints.org) | NOT PEER-REVIEWED | Posted: 27 August 2021 doi:10.20944/preprints202108.0520.v1

Based on this, we compared the miRNA population in the BALF and lung tissue-derived exosomes from healthy non-smokers, healthy smokers, and patients with COPD and IPF in several independent cohorts. Numerous studies have shown that circulating miRNAs are involved in the progression, development and severity of various diseases including COPD and IPF (6, 9, 11, 23-26). These are also considered to be known targets for biomarker development (27, 28). Hence, we compared the exosome-derived miRNA profiles amongst COPD and IPF patients with healthy individuals to identify miRNA signatures that might be unique to each of these distinct pathological conditions and help determine the progress of the pulmonary damage at an early stage.

Materials and Methods

Ethics/Approval

The human patients and the patients' data included in the study were procured from several agencies (described below) as human subjects were not directly involved in this work. The procurement of human lung tissues and BALF samples as deidentified samples was approved by the Materials Transfer Agreement and Procurement (Institutional Review Board, IRB), and Laboratory protocols by the Institutional Biosafety Committee (IBC) at the University of Rochester Medical Center, Rochester, NY. The project codes and dates of approval were as follow: Project Code: DRAI1 001 Protocol: 004, Date of approval and IRB/IBC approvals 2/11/2017 and 9/29/2017.

All the procedures/ protocols were carried per the guidelines and regulations specified by the University of Rochester, Rochester, NY. Other approvals include: (a) IRB study

 doi:10.20944/preprints202108.0520.v1

number 20080326 at the University of Miami, and (b) registered clinical trial (NCT04016181) and ethically approved by the University of Edinburgh (07/S1102/20) and NHS Lothian 2007/R/RES/02 by 14/06/2007. Additional samples were obtained from baseline measurements of Feasibility of Retinoids for the Treatment of Emphysema (FORTE) trial participants as described previously (29, 30).

Study population and Sample Collection

We employed bronchoalveolar lavage fluid (BALF) and lung tissues collected from healthy (Non-smokers and Smokers) and diseased (COPD and IPF) human subjects as samples for this study from 7 independent cohorts (**Table 1**). A total of 40 BALF samples and 32 lung tissue samples were chosen for this study from multiple sources. The majority of the BALF samples used in this study were procured from a commercial provider- BioIVT (Westbury, NY, USA). Rest of the BALF samples were provided by our collaborators- Dr. Michael Campos from Division of Pulmonary, Allergy, Critical Care at University of Miami, Dr. Hitendra Chand from Department of Immunology at Florida International University, Dr. Haseeb Siddiqi from Department of Cell Biology at SUNY Downstate Health Sciences University and Dr. Nikhil Hirani from Center of Inflammation research at Edinburgh University, UK. The samples procured from our collaborators were validated for their disease categories based on their spirometry and clinical status.

Likewise, the lung samples were procured from three sources; (a) commercially available resource for procurement of human tissue and organ- NDRI (National Disease Research Interchange), (b) NHLBI-funded bio-specimen repository- LTRC (Lung Tissue Research

Preprints (www.preprints.org) | NOT PEER-REVIEWED | Posted: 27 August 2021 doi:10.20944/preprints202108.0520.v1

Consortium), and (c) Department of Medicine and Pathology at the University of Helsinki Hospital, Finland as reported previously (31, 32).

All the subjects included in the study were above 21 years of age. Care was taken to include equal numbers of males and females in each subject group. A detailed characteristic of the BALF and Lung tissue samples used for this study is provided in **Table 1**.

BALF exosome isolation

We employed commercially available Plasma/Serum Exosome Purification and RNA Isolation Midi Kit from Norgen Biotek (Cat# 58500; Ontario, Canada) to isolate exosomes from human BALF samples. BALF exosomes were isolated as per manufacturer's protocol. In brief, 1 mL BALF sample was mixed with Nuclease-free water, ExoC Buffer and Slurry E; and incubated for 5 minutes at room temperature. Next, the solution was centrifuged at 2000 rpm for 5 min at room temperature and the supernatant was discarded. The slurry pellet was then resuspended in ExoR buffer and incubated for 10 min at room temperature. Thereafter the suspension was centrifuged at 8000 rpm for 2 min duration at room temperature and transferred to Mini Filter Spin column to elute the exosomal fraction. The eluted exosomes were then stored at -80^{0}C until further use.

Lung Tissue Exosome Isolation

The tissue exosomes were isolated using the protocol described by Dooner et al (2018) (33) with some modifications. In brief, 30-40 mg of lung tissue was chopped and lysed using 1X Liberase solution containing 0.01% DNase. The tube containing tissue lysate was left on an orbital shaker at 37^{0}C for 1-hour duration to allow complete digestion of

Preprints (www.preprints.org) | NOT PEER-REVIEWED | Posted: 27 August 2021 doi:10.20944/preprints202108.0520.v1

lung tissues. After 1-hour incubation, the tissue lysate was collected. The eluate was then centrifuged at 300 g for 10 min at 4^0C to remove cell debris. Next, the supernatant was transferred to fresh tube and centrifuged at 2000 g for 10 min at 4^0C. Again, the supernatant was transferred to a fresh tube and centrifuged at 10,000 g for 30 min at 4^0C to remove larger vesicles. After this, the supernatant was transferred to ultracentrifuge tubes and the exosomes were pelleted at 110,000g for 70 min at 4^0C using Optima Max-XP ultracentrifuge (Beckman Coulter, Brea, CA). At this stage, the supernatant was discarded and the pellet was resuspended in 1X PBS prior to filtering through 0.22µM filter. The filtrate was once again spun at 110,000g for 70 min at 4^0C. Finally, the supernatant was discarded and the pellet was re-suspended in 1mL 1X PBS. This contained freshly isolated tissue exosomes that were stored at -80^0C for future analysis.

Exosome Characterization

We employed Hitachi 7650 Analytical transmission electron microscopy (TEM) to visualize the isolated exosomes and nanoparticle tracking analysis (NanoSight NS300) to analyze the particle size and concentration as described earlier (12, 34).

We also used immunoblotting to identify exosomal markers from the isolated fraction to characterize the BALF and lung tissue derived exosomes. In brief, 20 ug of exosomal lysate was resolved on a 10% sodium dodecyl sulfate (SDS)-polyacrylamide gel and electroblotted onto nitrocellulose membranes. Membrane was blocked using 5% blocking buffer for 1 hr and thereafter probed overnight with antibodies for exosomal surface markers. The antibodies include-CD9 (Cat# ab92726), CD63 (Cat# ab134045) (Abcam, Cambridge, UK) and CD81 (Cat# EXOAB-CD81A-1) (SBI Biosciences, Palo Alto, CA).

Preprints (www.preprints.org) | NOT PEER-REVIEWED | Posted: 27 August 2021 doi:10.20944/preprints202108.0520.v1

The following days, the blots were washed and probed with appropriate secondary antibodies. Chemiluminescence was detected on the Bio-Rad ChemiDoc MP, Imaging system using the SuperSignal West Femto Maximum Sensitivity Substrate (Cat# 34096, Thermo Scientific, Waltham, MA).

Exosomal RNA extraction

Total RNA from BALF exosomes was isolated using Exosomal RNA isolation kit (Norgen Bioteck Corporation, Cat# 58000) as per the manufacturer's protocol. The detailed procedure has been published earlier (34).

Alternately, we used miRNeasy Mini Kit (Cat# 217004, Qiagen, Hilden, Germany) to isolate RNA from lung exosomes as per manufacturer's protocol. Briefly, 700 µl of QIAzol lysis buffer was mixed with 250 µl of exosomal fraction and the mix was homogenized using QIAshredder. The homogenate was then mixed with 140µl of chloroform to allow phase separation and the aqueous phase was transferred to a fresh tube. Thereafter, the RNA was precipitated using 100% ethanol and washed using RWT and RPE buffers provided with the kit. Finally, the RNA was eluted using RNase-free water and stored at -80^{0}C until further use. The RNA quality and quantity were checked using Agilent 2100 Bioanalyzer.

Library preparation

The isolated RNA samples were shipped to Norgen Biotek, Canada for library preparation, sequencing and data analyses. The library preparation was performed using the standard library preparation workflow of Norgen including 3' and 5' adapter ligation, followed by reverse transcription, indexing PCR and size selection using a 6% Novex

Preprints (www.preprints.org) | NOT PEER-REVIEWED | Posted: 27 August 2021 doi:10.20944/preprints202108.0520.v1

TBE Gel. In brief, Norgen Biotek Small RNA Library Prep Kit (Cat# 63600) was employed for library preparation making sure to use the same lot between each batch of samples.

Samples were quantified using both PicoGreen and Bioanalyzer. 6uL of high-quality total RNA was mixed with 3' adaptor and T4 RNA ligase 2 to set up a reaction for 3' Adaptor ligation per manufacturer's protocol. This was followed by the removal of excess 3' Adaptor and then 10-12 µl of final eluate was mixed with 5'Adaptor to set up a reaction for 5' Adaptor Ligation. Next, the reaction for cDNA synthesis was set using the obtained ligated product as input, per manufacturer's directions and incubated at 50^0C for 1 hour in a thermocycler. This was followed by PCR amplification and indexing as advised and cleanup of final indexed PCR product using NGS Reaction Cleanup Kit. After cleaning, the samples were run on a 6% Novex TBE Gel for 50 minutes at 140V. The adaptor dimer not containing any library was excised, and the sample was eluted from the gel and checked for quality as per the manual's instruction. At this stage, the library quality check was performed to estimate library size and concentration using Bioanalyzer. Samples were then pooled in equimolar ratios and further size selected using a 3% Agarose Gel cassette on the Pippin prep (Part # SAG-CDP3010). The pool was quantified by Bioanalyzer before starting the Next Generation Sequencing (NGS) run.

Next Generation Sequencing (NGS) and Data Analysis

We employed NextSeq 500/550 High Output Kit v2 for 75 cycles (Cat# 20024906, Illumina, San Diego, CA) to perform NGS on our pooled library. Per the manufacturer's directions the pooled library was denatured and diluted to the required concentration of 20pM for optimal cluster generation. Library was then applied onto the suitable flow-cell and sequenced using Illumina NextSeq 500 sequencing platform.

Preprints (www.preprints.org) | NOT PEER-REVIEWED | Posted: 27 August 2021 doi:10.20944/preprints202108.0520.v1

The raw sequence reads were analyzed by the team of bioinformaticians at Norgen using their advanced analysis pipeline for the processing of raw counts and alignment to endogenous genome and annotated transcriptome.

Gene Ontology and KEGG analyses

The gene ontology or GO (35) enrichment analysis was performed, through the examination of significant GO terms associated with the differentially expressed miRNAs for each comparison group. The analysis was performed by iteratively testing the enrichment of each annotated GO term correlated with the set of pre-selected differentially expressed genes (in our case, miRNAs) in a linear fashion. Individual enriched annotated GO terms were analyzed using a Fisher's exact test for both up-regulated and down-regulated genes in which GO terms with an FDR adjusted p-value threshold of 0.05 were reported as significantly relevant. The FDR is the false discovery rate generated using the Benjamini-Hochberg method, which adjusts the p-value based on the FDR. The analysis was performed separately on all three GO domains, i.e, biological process, molecular function and cellular component.

The KEGG (36) enrichment analysis was also performed to identify the differentially expressed genes within an associated pathway for various biological processes. The analysis was performed by testing the enrichment of each biological pathway with the associated gene (or miRNA) found within the set of pre-selected differentially expressed genes. Individually enriched pathways were then contrasted and compared between the two test groups using a Fisher's exact test for both up-regulated and down-regulated genes within the pre-selected set of differentially expressed genes. Biological pathways with an adjusted p-value below 0.05 were reported.

Preprints (www.preprints.org) | NOT PEER-REVIEWED | Posted: 27 August 2021 doi:10.20944/preprints202108.0520.v1

Statistical analysis

The miRNA data from various batches were normalized using trimmed mean of M-values (TMM) normalization method (37). The TMM normalized read counts were used for differential expression analysis. The Principal Component analysis (PCA) was plotted using the *ggfortify* function in R-software (version: 3.5.1) to produce a sample clustering plot based on miRNAs with the highest variation across all samples. The coefficient of variation (% CV) was calculated based on the $\log_2$ of TMM normalized data and then the 50 miRNAs with the highest %CV were selected and used to generate the PCA plot. The highest two components of variation were plotted on the x-axis (the first principal component, PCA1) and the y-axis (the second principal component, PCA2). Confidence ellipses and average center points were calculated and added for each sample group to further organize the biological groupings.

EdgeR statistical software package was used for DE analysis as described previously (38, 39). The Benjamini-Hochberg procedure was then used for adjusting the false discovery rate (FDR) (40). This allowed identifying the significant DE when comparing two groups. The DE was considered significant if log fold change of ≥ 1 or ≤ -1 at p- value and FDR of ≤ 0.05 was reported for the miRNA target. We used the *ggplot2* function in R software (version: 3.5.1) to plot volcano plots for illustrating a large number of miRNAs and displaying the particular miRNA targets with statistically significant differential expression.

Heat maps were generated using the *ComplexHeatmap* function in R-software (version: 3.5.1). The coefficient of variation (% CV) was calculated based on $\log_2$ of TMM

Preprints (www.preprints.org) | NOT PEER-REVIEWED | Posted: 27 August 2021 doi:10.20944/preprints202108.0520.v1

normalized data and then the 50 miRNAs with the highest %CV were selected and used to generate the heat map.

Kruskal-Wallis test was used to calculate significance for sample distribution.

Results

Characterization of BALF and lung-tissue derived exosomes

Exosomes are known to be involved with intercellular communication thus affecting the physiological processes in various tissues. Here, we analyzed the miRNA population from the BALF and lung tissue exosomes isolated from the non-smokers, smokers, and the patients with COPD or IPF. We first isolated the BALF and lung tissue-derived exosomes using the methods described earlier. We employed immunoblotting, nanoparticle tracking analysis (NTA: NanoSight 300), and transmission electron microscopy (TEM) to characterize the isolated exosomes. We first used NTA to determine the particle concentration, size, or distribution of exosomes in isolated samples from BALF and lung tissues. The lung-derived exosomes (avg. conc. = 2.38 $\pm$ 2.2 X 10^{11} particles/mL) had larger size (mean = 146.04 nm). On the other hand, the average size of the BALF-derived exosomes was ~89.85 nm (avg. conc. = 2.95 $\pm$ 2.2 X 10^{10} particles/mL) (Figs 1i & 2i). TEM analysis confirmed the morphology of isolated exosomes from BALF and lung tissue samples as shown in Figs 1ii & 2ii.

Finally, we used immunoblotting to study the presence of exosome surface markers (CD9, CD81 and CD63) in the isolated exosome fractions from BALF and lung tissues. We found enrichment of positive surface markers for BALF exosomes, such as CD9 and CD81 in the isolated exosome fractions (Fig 1iii, full blots in Suppl. Fig 1). Similarly, we

Preprints (www.preprints.org) | NOT PEER-REVIEWED | Posted: 27 August 2021 doi:10.20944/preprints202108.0520.v1

found abundance of positive surface markers for tissue exosomes- CD63 and CD81- in the exosome fractions from the lung tissues (Fig 2iii, full blots in Suppl. Fig 2). Overall, our results confirm the successful isolation of exosomes from human BALF and lung tissues in our study groups.

Batch variations in the exosome-derived miRNA expression profiles amongst the various study groups

We performed Principal Component analyses (PCA) to visualize the batch variations within the samples. Separate analyses were run for the BALF- and lung tissue-derived exosomes. The plot was generated by using 50 miRNAs with the highest component of variation among groups. Each sample group was clustered using a confidence ellipse as shown in the Fig 3. The PCA plot from lung-derived exosomal miRNAs showed a distinct clustering of the IPF patient samples as compared to the other three study groups, thus suggesting a unique transcriptomic identity of these lung-derived exosomes.

Pairwise comparison of BALF- and lung tissue-derived exosomal miRNAs expression profiles

Next, we generated volcano plots showing pairwise comparisons of the differential miRNA expression profiles between various experimental groups in BALF or lung tissue-derived exosomes (Figs 4&5). We plotted the $-\log_{10}$ of adjusted *p*-values on the Y-axis, and the $\log_2$ fold change between two experimental groups on the X-axis to generate a volcano plot. Fold changes greater than ±1 on the logarithmic (base2) scale of thus derived volcano plots were considered significant. miRNAs showing no significant fold change

Preprints (www.preprints.org) | NOT PEER-REVIEWED | Posted: 27 August 2021 doi:10.20944/preprints202108.0520.v1

were denoted with blue, while significantly up- or down-regulated miRNAs were denoted with green and red colored dots respectively.

Hierarchical clustering identified differentially expressed miRNAs in the BALF or lung-derived exosomes from non-smokers, smokers, patients of COPD and IPF

We generated heat maps showing the top 50 differentially expressed miRNAs from the BALF and lung tissue-derived exosomes from NS vs Sm, NS vs COPD, NS vs IPF and Sm vs COPD as shown in Figs 6 &7 . Each miRNA is depicted in the individual row of the heat map while the color scale represents the relative expression level as denoted in the scale bar alongside. A detailed information about the significantly altered miRNAs with their respective p-values and biological significance has been listed in Supplementary Tables 1&2. In brief, the following observations were made on comparing the various experimental pairs:

Non-smokers vs Smokers: We did not detect any significant differentially expressed miRNA in the BALF-derived exosomes from smokers and non-smokers. Similarly, no significant variation was observed on comparing the miRNA population from lung tissue-derived exosomes from smokers and non-smokers.

Non-smokers vs COPD: On comparing the BALF derived exosomal miRNAs from non-smokers and COPD patients, we found three significant differentially expressed miRNAs. Of these, two (miR-320b and miR-22-3p) were significantly upregulated, while one (miR-423-5p) was significantly downregulated in the BALF-derived exosomes from COPD patients as compared to the non-smoking controls. In contrast, we demonstrated

Preprints (www.preprints.org) | NOT PEER-REVIEWED | Posted: 27 August 2021 doi:10.20944/preprints202108.0520.v1

significant downregulation of one (miR-122-5p) exosomal miRNA in the lung-tissues of COPD patients as compared to non-smokers.

Smoker vs COPD: We observed significant downregulation of miR-100-5p in the BALF-derived exosomes from COPD patients in comparison to those from healthy smokers.

Similarly, on comparing the lung-derived exosomes from these two study groups we found a significant downregulation of one miRNA. We noticed a significant downregulation of miR-122-5p in the exosomes derived from the lungs of COPD patients as compared to healthy smokers. Interestingly, the same miRNA was found to be downregulated on comparing the miRNA population from the lung-derived exosomes from COPD patients and non-smokers.

Non-smokers vs IPF: Our results showed a distinct miRNA signature in the BALF and lung tissue-derived exosomes from IPF patients as compared to non-smoking controls. A total of nine differentially expressed miRNAs were identified from the BALF-derived exosomes of IPF patients as compared to healthy non-smoking controls. Of the 9, five (miR-375-3p, miR-200a-3p, miR-200b-3p, miR-141-3p, and miR-423-5p) miRNAs were significantly downregulated; while four (miR-22-3p, miR-320a-3p, miR-320b, and miR-24-3p) were upregulated in the BALF of IPF patients.

Interestingly, we found 55 (26 upregulated and 29 downregulated) differentially expressed miRNAs in the lung-derived exosomes from lungs of IPF patients as compared to non-smoking controls.

GO enrichment and KEGG analyses differentially expressed miRNAs from BALF and lung-derived exosomes in COPD and IPF patients

Preprints (www.preprints.org) | NOT PEER-REVIEWED | Posted: 27 August 2021 doi:10.20944/preprints202108.0520.v1

To understand the potential functions of the differentially expressed miRNAs in COPD and IPF patients, we performed GO enrichment covering three major domains- biological process, cellular compartment and molecular function. GO term annotation of differentially altered miRNAs in BALF-derived exosomes from COPD patients as compared to healthy non-smokers and smokers resulted in enrichment of terms including: post-translational protein modification, ubiquinone biosynthetic process, cellular component organization, membrane enclosed lumen, clathrin-coated vesicle, mitochondrial matrix, protein binding, protein heterodimerization and transferase activity. The regulatory pathway annotation by KEGG enrichment analyses showed representation of pathways involved in terpenoid backbone biosynthesis, cAMP signaling, cellular senescence and chemokine signaling amongst COPD patients. However, none of these pathways was significantly over-represented in our analyses. GO annotation for miRNA population obtained from IPF patient BALF resulted in enrichment of terms including, lipid transport, mesenchymal cell development, chromatin, mitochondria, lysosome, R-SMAD binding and ATPase activity. The KEGG analyses for this subject group showed 80% overlap with the pathways enriched amongst COPD patients. Interestingly, however, we found a significant overrepresentation of pathways regulating glycosaminoglycan biosynthesis ($p=0.028$) in the BALF-derived exosomes from IPF patients.

GO annotation of differentially regulated miRNAs from lung derived exosomes was conducted separately. We found enrichment of terms like, blood vessel morphogenesis, angiogenesis, transmembrane signaling receptor activity, G protein-coupled receptor activity, calcium mediated signaling and calcineurin-NFAT signaling cascade in lung-

 doi:10.20944/preprints202108.0520.v1

derived exosomes from COPD patients as compared to healthy individuals (non-smokers and smokers). Contrarily, GO terms including, plasma membrane bounded cell projection organization, chemical homeostasis, G protein-coupled receptor activity, positive regulation of phospholipase C activity, MHC class II protein complex signaling, GTPase activator activity, and positive regulation of non-membrane spanning protein tyrosine kinase activity were found to be enriched on analyzing differentially expressed miRNAs from lung-derived exosomes in IPF patients. KEGG enrichment analyses showed overrepresentation of pathways regulating apoptosis, asthma, and cGMP-PKG signaling pathway, amongst others in COPD patients. However, none of these regulatory pathways were significantly represented. Contrarily, KEGG enrichment analyses of miRNA profile from IPF patients identified representation of 40 pathways, of which 12 were significantly represented in the miRNA population from the lung-derived exosomes from IPF patients.

Tables 2-5 provide an account of the GO enrichment and KEGG analyses results for our comparisons of various subject groups in this study. Only selected pathways has been represented in the Tables.

Discussion

The role of exosomes in lung diseases has gained increasing attention in recent times due to their role in influencing intercellular communication. These are 50-150 nm in diameter, membrane-bound vesicles that contain protein, DNA, mRNA, microRNA (miRNA) and small non-coding RNAs to regulate pleiotropic functions(41). Recent studies suggest that exosomes mediate cellular crosstalk in lung microenvironment and

 doi:10.20944/preprints202108.0520.v1

that cigarette smoke-induced exosomes promote myofibroblast differentiation in primary lung fibroblasts (21, 22). In addition, activated exosomes (due to cigarette smoke or disease conditions) result in macrophage polarization and matrix destruction in mouse models (42, 43). These studies implicate that exosomes affect cell-to-cell signaling in tobacco smoke-related disorders.

In this respect, inhalation of toxic agents from tobacco smoke might result in irreparable airway injury leading to various lung diseases like COPD and IPF. While the etiology/cause of each of these diseases might be environmental factors, the disease pathologies are distinct (41). Therefore, we were interested in understanding if the exosomal population and the exosome-derived miRNA signatures from BALF and lung tissues of non-smokers, smokers, COPD patients and IPF patients are unique and can be developed into effective biomarkers for the clinical diagnosis of respective pathologies.

Results from next generation sequencing revealed no significant differentially expressed miRNAs in the BALF or lung-derived exosomes from heathy smokers and non-smokers. This suggests that smoking status alone does not affect the exosome-mediated signaling in healthy individuals. However, we found a distinct variation in the miRNA populations from BALF and lung tissue-derived exosomes from COPD patients in comparison to healthy non-smokers. We found a 3-fold downregulation in the expression of miR-423-5p in the BALF-derived exosomes from COPD patients as compared to healthy non-smoking controls. Of note, miR-423-5p is known to be involved in the regulation of apoptosis and extracellular matrix degradation in human nucleus pulposus cells (44). Contrary to our findings, Molina-Pinelo *et al* (2014) identified increased expression of miR-423-5p in the BALF collected from COPD patients as compared to the control group. However, it is

 doi:10.20944/preprints202108.0520.v1

important to mention here that the control group included in this study comprised of a few ex- smokers and they did not look at the exosome-derived miRNA from BALF (45). So taken together, it can be concluded that miR-423-5p is crucial in COPD and must be studied further to understand its potential role in the pathophysiology of COPD.

Further, we observed two-fold increase in the expression of miR-320b and miR-22-3p in the BALF-derived exosomes from COPD patients as compared to the non-smoking controls. Previous study by our group identified upregulation of both miR-320b and miR-22-3p in the peripheral blood-derived exosomes of COPD patients (11), thus indicating significant role of these miRNAs in regulating the disease phenotype. miR-320b is the negative regulator of mitochondrial mediator, TP53-regulated inhibitor of apoptosis (TRIAP1), and has been previously shown to be upregulated in the peripheral blood nuclear cells (PBMCs) from COPD patients (46, 47). Similarly, miR-22-3p is reported to inhibit HDAC4 to promote Th17-mediated emphysema in cigarette smoke (4 month)-exposed C57Bl/6 mice lungs (48). Serum levels of miR-22-3p are known to be increased amongst COPD patients based on their history of smoking, thus revealing the crucial nature of this miRNA in the progression of the disease (49).

On comparing the miRNA expression of lung tissue-derived exosomes from COPD patients and non-smokers, we observed 3-fold downregulation of miR-122-5p in the lungs of COPD patients as compared to healthy non-smoking controls. Importantly, we further observed a 5-fold decrease in the expression of miR-122-5p on comparing miRNA population from lung-derived exosomes from COPD patients versus healthy smokers. Our results are in accordance with previous literature (50-52). For instance, Zhu *et al* (2020) demonstrated the downregulation of miR-122-5p in the sputum and plasma of

 doi:10.20944/preprints202108.0520.v1

COPD patients and proved that it functions as a negative regulator of IL-17A production (50). It is pertinent to mention here that though we did not find any commonly altered miRNAs in the exosomes from BALF or lung tissues of COPD patients, we found links that associate miRNA-mediated modulation of IL17-signalling amongst the diseased individual. The role of IL-17 in the disease pathology of COPD is rapidly emerging and is known to play an important role in the regulation of chronic inflammation and emphysema in COPD (53). Hence, our findings identify the upstream regulators of this pathway that could possibly alter the IL17-mediated inflammation in patients with advancing disease.

Next, we identified significant downregulation of miR-100-5p in the BALF-derived exosomes from COPD patients as compared to healthy smokers. Functionally, miR-100 has been linked to the regulation of epithelial-mesenchymal transition (EMT), apoptosis and inflammation (54, 55). Furthermore, Akbas and colleagues have demonstrated downregulation of miR-100-5p in the serum of COPD patients when compared to healthy smokers, which is in accordance to our study results (56).

The differentially expressed miRNA population from BALF and lung tissue-derived exosomes in COPD and IPF was very distinct in our study. We found five significantly downregulated (miR-200a-3p, miR-200b-3p, miR-141-3p, miR-375-3p, and miR-423-3p) whereas four significantly upregulated (miR-320a-3p, miR-320b, miR-22-3p and miR-24-3p) miRNAs in the BALF-derived exosomes from IPF patients. Of these, miR-423-3p and miR-320b were found to be significantly dysregulated amongst COPD patients as well. Of note, existing reports suggest a role of miR-200 in the pathogenesis of IPF (57, 58). It has been shown that miR-200 promotes TGF-β1-induced EMT in normal cells and its downregulation results in fibrogenic phenotype in IPF (57). To our knowledge, there is no

existing literature associating miR-141-3p, miR-22-3p and miR-24-3p with IPF. Thus, we for the first time identify the association of these miRs with the disease pathogenesis in IPF.

We found 55 differentially expressed miRNAs in the lung-derived exosomes from IPF patients when compared to non-smokers. Of these, many including miR514-3p, miR-122-5p, miR-10b-5p, miR-139b-3p, miR-582-5p, miR-889-3p, miR-1-3p, miR-148a-3p and miR-151b, have never been reported with IPF. Our study for the first time reports the correlation of the dysregulated expression of these miRNAs in the lung derived exosomes from IPF patients. Of note, we observed a three-fold increase in the expression of miR-506-3p in the lung-derived exosomes from IPF patients as compared to the healthy non-smoking controls. Previous work by Zhu et al (2019) reported that miR-506-3p targets p65 subunit of NF-κB to induce apoptosis and inflammation in experimental mice model for IPF. This study concluded that miR-506-3p is a regulator of lung fibrosis (59). Our results provide clinical evidence suggesting a crucial role of this miRNA in the pathophysiology of IPF in humans. Similarly, accumulating evidence support the role of miR-21-5p in the disease progression of IPF (60-62). Further, the expression of miR-21-5p is controlled by the levels of TGF-β family proteins and SMADs, both of which are key regulators in the etiology of fibrosis (63).

Our study had some limitations. Firstly, the sample size for each of the study groups was quite small (n=8-16). In addition, due to non-availability of age- and gender-matched individuals in our cohorts, we were unable to normalize for the gender and age-specific bias in our results. Further limitations were the non-availability of non-smokers/never-smokers and limited information regarding the spirometry, pack-years and smoking

Preprints (www.preprints.org) | NOT PEER-REVIEWED | Posted: 27 August 2021 doi:10.20944/preprints202108.0520.v1

history of all the subjects included in this study, which may have affected the final interpretation of our findings.

Conclusions

Overall, this is the first study that compares the BALF and lung tissue-derived exosomal miRNAs from IPF and COPD patients with healthy subjects to suggest the unique miRNA signatures that could develop as a biomarker to identify the disease progression of these pulmonary conditions. Future studies will be designed to validate the findings from this work and to understand the role of exosomal miRNAs in affecting the disease development, progression and severity in COPD and IPF.

List of Abbreviations:

COPD: Chronic Obstructive Pulmonary disease
IPF: Idiopathic Pulmonary disease
TEM: Transmission Electron Microscopy
NGS: Next Generation sequencing
miRNA: micro RNA
BALF: Bronchoalveolar Lavage fluid
EMT: epithelial-mesenchymal transition

Acknowledgements: The authors would like to acknowledge Drs. Isaac Sundar and Dongmei Li for their scientific inputs. We would further like to thank Sarah McNamara, research nurse at Centre for Inflammation Research, University of Edinburgh for providing patient care during sample collection for this study. We would like to acknowledge Dr. Robert Foronjy, Associate Professor at SUNY Downstate Health Sciences University for

for clinical support for some of the BALF samples included in the study. We would also like to acknowledge Dr. Ashokkumar Srinivasan for his assistance in optimization of study protocol.

Declarations: The authors have declared that no competing interests exist.

Funding: The National Institutes of Health (NIH) HL137738, HL133404 and HL135613 supported this work.

Role of the Funder/Sponsor: The content is solely the responsibility of the authors and does not necessarily represent the official views of the NIH.

Disclaimer: None

Meeting Presentation: None

Additional Contributions: None

Competing interests: The authors have no competing interests.

Data Availability: All the data included in this manuscript is available online and is free to access to all readers. The NGS data and/or analyzed files during the current study are available at Gene Expression Omnibus accession number GSE180651 (https://www.ncbi.nlm.nih.gov/geo/query/acc.cgi?acc=GSE180651). Data available date: August 15-2021.

Availability of data and materials: All authors confirm the availability of data and materials online/free access to readers.

Authors Contribution: GK and KPM designed and conducted the experiments, GK and IR wrote, edited and/or revised the manuscript. GK was responsible for data curation, IR

conceptually designed the overall experiments and manuscript, and acquired funding. MC, HSC, FL, NK, MAH provided BALF and/or lung tissues and edited the manuscript.

References

1. Sousa C, Rodrigues M, Carvalho A, Viamonte B, Cunha R, Guimarães S, et al. Diffuse smoking-related lung diseases: insights from a radiologic-pathologic correlation. Insights Imaging. 2019;10(1):73-.
2. Ryu JH, Colby TV, Hartman TE, Vassallo R. Smoking-related interstitial lung diseases: a concise review. European Respiratory Journal. 2001;17(1):122.
3. Chilosi M, Poletti V, Rossi A. The pathogenesis of COPD and IPF: distinct horns of the same devil? Respir Res. 2012;13(1):3-.
4. Devine JF. Chronic obstructive pulmonary disease: an overview. Am Health Drug Benefits. 2008;1(7):34-42.
5. Glassberg MK. Overview of idiopathic pulmonary fibrosis, evidence-based guidelines, and recent developments in the treatment landscape. The American journal of managed care. 2019;25(11 Suppl):S195-s203.
6. O'Farrell HE, Yang IA. Extracellular vesicles in chronic obstructive pulmonary disease (COPD). J Thorac Dis. 2019;11(Suppl 17):S2141-S54.
7. Wang N, Wang Q, Du T, Gabriel ANA, Wang X, Sun L, et al. The Potential Roles of Exosomes in Chronic Obstructive Pulmonary Disease. Front Med (Lausanne). 2021;7:618506-.
8. Minnis P, Kane R, Anglin R, Walsh S, Worrel J, Khan F, et al. Serum exosomes from IPF patients display a fibrotic miRNA profile that correlates to clinical measures of disease severity. European Respiratory Journal. 2015;46(suppl 59):PA3845.
9. Njock M-S, Guiot J, Henket MA, Nivelles O, Thiry M, Dequiedt F, et al. Sputum exosomes: promising biomarkers for idiopathic pulmonary fibrosis. Thorax. 2019;74(3):309.
10. Mohan A, Agarwal S, Clauss M, Britt NS, Dhillon NK. Extracellular vesicles: novel communicators in lung diseases. Respir Res. 2020;21(1):175.
11. Sundar IK, Li D, Rahman I. Small RNA-sequence analysis of plasma-derived extracellular vesicle miRNAs in smokers and patients with chronic obstructive pulmonary disease as circulating biomarkers. Journal of extracellular vesicles. 2019;8(1):1684816.
12. Sundar IK, Li D, Rahman I. Proteomic Analysis of Plasma-Derived Extracellular Vesicles in Smokers and Patients with Chronic Obstructive Pulmonary Disease. ACS Omega. 2019;4(6):10649-61.
13. Sundar IK, Yao H, Rahman I. Oxidative stress and chromatin remodeling in chronic obstructive pulmonary disease and smoking-related diseases. Antioxidants & redox signaling. 2013;18(15):1956-71.
14. Lerner CA, Sundar IK, Rahman I. Mitochondrial redox system, dynamics, and dysfunction in lung inflammaging and COPD. The international journal of biochemistry & cell biology. 2016;81(Pt B):294-306.
15. Takahashi T, Kobayashi S, Fujino N, Suzuki T, Ota C, He M, et al. Increased circulating endothelial microparticles in COPD patients: a potential biomarker for COPD exacerbation susceptibility. Thorax. 2012;67(12):1067-74.
16. Lacedonia D, Carpagnano GE, Trotta T, Palladino GP, Panaro MA, Zoppo LD, et al. Microparticles in sputum of COPD patients: a potential biomarker of the disease? International journal of chronic obstructive pulmonary disease. 2016;11:527-33.

17. Tan DBA, Armitage J, Teo TH, Ong NE, Shin H, Moodley YP. Elevated levels of circulating exosome in COPD patients are associated with systemic inflammation. Respiratory medicine. 2017;132:261-4.
18. Eltom S, Dale N, Raemdonck KR, Stevenson CS, Snelgrove RJ, Sacitharan PK, et al. Respiratory infections cause the release of extracellular vesicles: implications in exacerbation of asthma/COPD. PloS one. 2014;9(6):e101087.
19. Gordon C, Gudi K, Krause A, Sackrowitz R, Harvey BG, Strulovici-Barel Y, et al. Circulating endothelial microparticles as a measure of early lung destruction in cigarette smokers. American journal of respiratory and critical care medicine. 2011;184(2):224-32.
20. Shen Y, Wang L, Wu Y, Ou Y, Lu H, Yao X. A novel diagnostic signature based on three circulating exosomal mircoRNAs for chronic obstructive pulmonary disease. Exp Ther Med. 2021;22(1):717-.
21. Fujita Y, Araya J, Ito S, Kobayashi K, Kosaka N, Yoshioka Y, et al. Suppression of autophagy by extracellular vesicles promotes myofibroblast differentiation in COPD pathogenesis. J Extracell Vesicles. 2015;4:28388-.
22. Bartel S, Deshane J, Wilkinson T, Gabrielsson S. Extracellular Vesicles as Mediators of Cellular Cross Talk in the Lung Microenvironment. Front Med (Lausanne). 2020;7:326-.
23. Salimian J, Mirzaei H, Moridikia A, Harchegani AB, Sahebkar A, Salehi H. Chronic obstructive pulmonary disease: MicroRNAs and exosomes as new diagnostic and therapeutic biomarkers. Journal of research in medical sciences : the official journal of Isfahan University of Medical Sciences. 2018;23:27.
24. Savarimuthu Francis SM, Davidson MR, Tan ME, Wright CM, Clarke BE, Duhig EE, et al. MicroRNA-34c is associated with emphysema severity and modulates SERPINE1 expression. BMC genomics. 2014;15:88.
25. Guiot J, Njock M-S, Henket M, Nivelles O, Louis R, Struman I. Sputum exosomal microRNAs in IPF. European Respiratory Journal. 2018;52(suppl 62):OA2119.
26. Liu B, Li R, Zhang J, Meng C, Zhang J, Song X, et al. MicroRNA-708-3p as a potential therapeutic target via the ADAM17-GATA/STAT3 axis in idiopathic pulmonary fibrosis. Experimental & Molecular Medicine. 2018;50(3):e465-e.
27. Chen YW, Leung JM, Sin DD. A Systematic Review of Diagnostic Biomarkers of COPD Exacerbation. PloS one. 2016;11(7):e0158843.
28. Shaw JG, Vaughan A, Dent AG, O'Hare PE, Goh F, Bowman RV, et al. Biomarkers of progression of chronic obstructive pulmonary disease (COPD). J Thorac Dis. 2014;6(11):1532-47.
29. Roth MD, Connett JE, D'Armiento JM, Foronjy RF, Friedman PJ, Goldin JG, et al. Feasibility of retinoids for the treatment of emphysema study. Chest. 2006;130(5):1334-45.
30. Agudelo CW, Kumley BK, Area-Gomez E, Xu Y, Dabo AJ, Geraghty P, et al. Decreased surfactant lipids correlate with lung function in chronic obstructive pulmonary disease (COPD). PloS one. 2020;15(2):e0228279.
31. Maremanda KP, Sundar IK, Li D, Rahman I. Age-Dependent Assessment of Genes Involved in Cellular Senescence, Telomere, and Mitochondrial Pathways in Human Lung Tissue of Smokers, COPD, and IPF: Associations With SARS-CoV-2 COVID-19 ACE2-TMPRSS2-Furin-DPP4 Axis. 2020;11(1356).
32. Sundar IK, Yin Q, Baier BS, Yan L, Mazur W, Li D, et al. DNA methylation profiling in peripheral lung tissues of smokers and patients with COPD. Clinical epigenetics. 2017;9:38.
33. Dooner MS, Stewart C, Deng Y, Papa E, Pereira M, Del Tatto M, et al. Daily rhythms influence the ability of lung-derived extracellular vesicles to modulate bone marrow cell phenotype. PloS one. 2018;13(11):e0207444.
34. Singh K, Maremanda K, Li D, Rahman I. Exosomal microRNAs are novel circulating biomarkers in cigarette,waterpipe smokers, E-cigarette users and dual smokers. BMC Medical Genomics. 2020.
35. Ashburner M, Ball CA, Blake JA, Botstein D, Butler H, Cherry JM, et al. Gene Ontology: tool for the unification of biology. Nature Genetics. 2000;25(1):25-9.

36. Kanehisa M, Goto S, Kawashima S, Nakaya A. The KEGG databases at GenomeNet. Nucleic acids research. 2002;30(1):42-6.
37. Robinson MD, Oshlack A. A scaling normalization method for differential expression analysis of RNA-seq data. Genome biology. 2010;11(3):R25.
38. Robinson MD, Smyth GK. Moderated statistical tests for assessing differences in tag abundance. Bioinformatics (Oxford, England). 2007;23(21):2881-7.
39. Robinson MD, McCarthy DJ, Smyth GK. edgeR: a Bioconductor package for differential expression analysis of digital gene expression data. Bioinformatics (Oxford, England). 2010;26(1):139-40.
40. Benjamini Y, Hochberg Y. Controlling the False Discovery Rate: A Practical and Powerful Approach to Multiple Testing. 1995;57(1):289-300.
41. Fujita Y, Kosaka N, Araya J, Kuwano K, Ochiya T. Extracellular vesicles in lung microenvironment and pathogenesis. Trends in Molecular Medicine. 2015;21(9):533-42.
42. Wang L, Chen Q, Yu Q, Xiao J, Zhao H. Cigarette smoke extract-treated airway epithelial cells-derived exosomes promote M1 macrophage polarization in chronic obstructive pulmonary disease. International immunopharmacology. 2021;96:107700.
43. Genschmer KR, Russell DW, Lal C, Szul T, Bratcher PE, Noerager BD, et al. Activated PMN Exosomes: Pathogenic Entities Causing Matrix Destruction and Disease in the Lung. Cell. 2019;176(1-2):113-26.e15.
44. Xu H, Ji L, Yu C, Chen Q, Ge Q, Lu Y. MiR-423-5p Regulates Cells Apoptosis and Extracellular Matrix Degradation via Nucleotide-Binding, Leucine-Rich Repeat Containing X1 (NLRX1) in Interleukin 1 beta (IL-1β)-Induced Human Nucleus Pulposus Cells. Med Sci Monit. 2020;26:e922497-e.
45. Molina-Pinelo S, Pastor MD, Suarez R, Romero-Romero B, González De la Peña M, Salinas A, et al. MicroRNA clusters: dysregulation in lung adenocarcinoma and COPD. European Respiratory Journal. 2014;43(6):1740.
46. Dang X, Qu X, Wang W, Liao C, Li Y, Zhang X, et al. Bioinformatic analysis of microRNA and mRNA Regulation in peripheral blood mononuclear cells of patients with chronic obstructive pulmonary disease. Respir Res. 2017;18(1):4-.
47. Li Y, Tang X, He Q, Yang X, Ren X, Wen X, et al. Overexpression of Mitochondria Mediator Gene TRIAP1 by miR-320b Loss Is Associated with Progression in Nasopharyngeal Carcinoma. PLOS Genetics. 2016;12(7):e1006183.
48. Lu W, You R, Yuan X, Yang T, Samuel ELG, Marcano DC, et al. The microRNA miR-22 inhibits the histone deacetylase HDAC4 to promote T(H)17 cell-dependent emphysema. Nat Immunol. 2015;16(11):1185-94.
49. Velasco-Torres Y, Ruiz V, Montaño M, Pérez-Padilla R, Falfán-Valencia R, Pérez-Ramos J, et al. Participation of the miR-22-HDAC4-DLCO Axis in Patients with COPD by Tobacco and Biomass. Biomolecules. 2019;9(12):837.
50. Zhu K, Zhou S, Xu A, Sun L, Li M, Jiang H, et al. Microbiota Imbalance Contributes to COPD Deterioration by Enhancing IL-17a Production via miR-122 and miR-30a. Mol Ther Nucleic Acids. 2020;22:520-9.
51. Osei ET, Florez-Sampedro L, Timens W, Postma DS, Heijink IH, Brandsma C-A. Unravelling the complexity of COPD by microRNAs: it's a small world after all. European Respiratory Journal. 2015;46(3):807.
52. Qian Y, Mao Z, Shi Y, Liu Z, Cao Q, Zhang Q. Comprehensive Analysis of miRNA-mRNA-lncRNA Networks in Non-Smoking and Smoking Patients with Chronic Obstructive Pulmonary Disease. Cellular Physiology and Biochemistry. 2018;50(3):1140-53.
53. Rich HE, Alcorn JF. IL-17 Strikes a Chord in Chronic Obstructive Pulmonary Disease Exacerbation. American journal of respiratory cell and molecular biology. 2018;58(6):669-70.

54. Liang Y, Zhao G, Tang L, Zhang J, Li T, Liu Z. MiR-100-3p and miR-877-3p regulate overproduction of IL-8 and IL-1β in mesangial cells activated by secretory IgA from IgA nephropathy patients. Experimental cell research. 2016;347(2):312-21.
55. Han W, Ren X, Yang Y, Li H, Zhao L, Lin Z. microRNA-100 functions as a tumor suppressor in non-small cell lung cancer via regulating epithelial-mesenchymal transition and Wnt/β-catenin by targeting HOXA1. Thoracic cancer. 2020;11(6):1679-88.
56. Akbas F, Coskunpinar E, Aynaci E, Oltulu YM, Yildiz P. Analysis of serum micro-RNAs as potential biomarker in chronic obstructive pulmonary disease. Experimental lung research. 2012;38(6):286-94.
57. Yang S, Banerjee S, de Freitas A, Sanders YY, Ding Q, Matalon S, et al. Participation of miR-200 in pulmonary fibrosis. Am J Pathol. 2012;180(2):484-93.
58. Moimas S, Salton F, Kosmider B, Ring N, Volpe MC, Bahmed K, et al. miR-200 family members reduce senescence and restore idiopathic pulmonary fibrosis type II alveolar epithelial cell transdifferentiation. ERJ Open Research. 2019;5(4):00138-2019.
59. Zhu M, An Y, Zhang X, Wang Z, Duan H. Experimental pulmonary fibrosis was suppressed by microRNA-506 through NF-kappa-mediated apoptosis and inflammation. Cell and Tissue Research. 2019;378(2):255-65.
60. Makiguchi T, Yamada M, Yoshioka Y, Sugiura H, Koarai A, Chiba S, et al. Serum extracellular vesicular miR-21-5p is a predictor of the prognosis in idiopathic pulmonary fibrosis. Respir Res. 2016;17(1):110-.
61. Ma X, Kumar M, Choudhury SN, Becker Buscaglia LE, Barker JR, Kanakamedala K, et al. Loss of the miR-21 allele elevates the expression of its target genes and reduces tumorigenesis. Proceedings of the National Academy of Sciences of the United States of America. 2011;108(25):10144-9.
62. Li YF, Jing Y, Hao J, Frankfort NC, Zhou X, Shen B, et al. MicroRNA-21 in the pathogenesis of acute kidney injury. Protein & cell. 2013;4(11):813-9.
63. Davis BN, Hilyard AC, Lagna G, Hata A. SMAD proteins control DROSHA-mediated microRNA maturation. Nature. 2008;454(7200):56-61.

Tables

Table1: Clinical characteristics of study subjects

Characteristics	Non-Smokers	Smokers	COPD/Emphysema	IPF	p-value*
BALF					
N	8	8	16	8	
Age (yrs), mean (SD)	49.6 (17.3)	57.4 (8.9)	65.9 (13.3)	76.5 (11.4)	0.0029
Gender					0.2952
Male n (%)	3 (37.5)	2 (25)	7 (38.9)	6 (75)	
N/A	_	_	2	_	
Smoking Status					0.9719
Current Smoker	-	6	2	-	

Ex-smoker	-	2	6	4	
N/A	-	-	7	-	
Lung Tissues					
N	8	8	8	8	
Age (yrs), mean (SD)	48.3 (16.3)	53.8 (15.4)	59.1 (9.9)	68.9 (9.6)	0.0688
Gender					0.981
Male n (%)	4 (50)	6 (75)	3 (37.5)	5 (62.5)	
N/A	2	1	-	-	
Smoking Status					>0.9999
Current Smoker	-	7	2	-	
Ex-smoker	3	1	4	6	
N/A	-	-	1	-	

*: Kruskal-Wallis test

Table 2: GO Enrichment Analysis of differentially expressed miRNAs in BALF-derived exosomes

ID	Term	Ontology	n	p-value*
NS vs COPD				
GO:0016043	Cellular component organization	BP	17	0.183535762
GO:0071840	Cellular component organization or biogenesis	BP	17	0.183535762
GO:0061024	membrane organization	BP	3	0.149797571
GO:0051259	protein complex oligomerization	BP	3	0.149797571
GO:0006720	isoprenoid metabolic process	BP	2	0.101214575
GO:0051186	cofactor metabolic process	BP	2	0.101214575
GO:0051188	cofactor biosynthetic process	BP	2	0.101214575
GO:0051262	protein tetramerization	BP	2	0.101214575
GO:0008299	isoprenoid biosynthetic process	BP	2	0.101214575
GO:0006732	coenzyme metabolic process	BP	1	0.051282051
GO:0009108	coenzyme biosynthetic process	BP	1	0.051282051
GO:0006733	oxidoreduction coenzyme metabolic process	BP	1	0.051282051
GO:0043687	post-translational protein modification	BP	1	0.051282051
GO:1901661	quinone metabolic process	BP	1	0.051282051
GO:0042181	ketone biosynthetic process	BP	1	0.051282051
GO:0051290	protein heterotetramerization	BP	1	0.051282051
GO:0051291	protein heterooligomerization	BP	1	0.051282051
GO:0006743	ubiquinone metabolic process	BP	1	0.051282051
GO:0006744	ubiquinone biosynthetic process	BP	1	0.051282051

Preprints (www.preprints.org) | NOT PEER-REVIEWED | Posted: 27 August 2021 doi:10.20944/preprints202108.0520.v1

GO:1901663	quinone biosynthetic process	BP	1	0.051282051
GO:0031974	membrane-enclosed lumen	CC	11	0.007422402
GO:0070013	intracellular organelle lumen	CC	11	0.007422402
GO:0030659	cytoplasmic vesicle membrane	CC	5	0.24291498
GO:0044431	Golgi apparatus part	CC	5	0.24291498
GO:0044429	mitochondrial part	CC	3	0.149797571
GO:1902494	catalytic complex	CC	3	0.149797571
GO:1990234	transferase complex	CC	2	0.101214575
GO:0005788	endoplasmic reticulum lumen	CC	2	0.101214575
GO:0030133	transport vesicle	CC	2	0.101214575
GO:0005802	trans-Golgi network	CC	1	0.051282051
GO:0030135	coated vesicle	CC	1	0.051282051
GO:0030136	clathrin-coated vesicle	CC	1	0.051282051
GO:0030662	coated vesicle membrane	CC	1	0.051282051
GO:0030665	clathrin-coated vesicle membrane	CC	1	0.051282051
GO:0005759	mitochondrial matrix	CC	1	0.051282051
GO:0016765	transferase activity, transferring alkyl or aryl (other than methyl) groups	MF	2	0.101214575
GO:0046982	protein heterodimerization	MF	1	0.051282051
GO:0000010	trans-hexaprenyltranstransferase activity	MF	1	0.051282051
GO:0050347	trans-octaprenyltranstransferase activity	MF	1	0.051282051
Sm Vs COPD				
GO:0007623	ciracdian rhythm	BP	4	0.114285714
GO:0048511	rhythmic process	BP	4	0.114285714
GO:1901566	organonitrogen compound biosynthetic process	BP	4	0.114285714
GO:1901135	carbohydrate derivative metabolic process	BP	3	0.085714286
GO:1901137	carbohydrate derivative biosynthetic process	BP	2	0.057142857
GO:0006022	aminoglycan metabolic process	BP	1	0.028571429
GO:0006023	aminoglycan biosynthetic process	BP	1	0.028571429
GO:0006024	glycosaminoglycan biosynthetic process	BP	1	0.028571429
GO:0005794	glycosaminoglycan metabolic process	BP	1	0.028571429
GO:0030203	bounding membrane of organelle	CC	8	0.228571429
GO:0001904	organelle subcompartment	CC	6	0.171428571
GO:0044431	Golgi apparatus	CC	6	0.171428571
GO:0098588	Golgi subcompartment	CC	5	0.142857143
GO:0098791	Golgi membrane	CC	4	0.114285714
GO:0016740	transferase activity	MF	5	0.142857143
GO:0016782	transferase activity, transferring sulphur-containing groups	MF	1	0.028571429
GO:0008146	sulphotransferase activity	MF	1	0.028571429
GO:0034483	heparan sulphate sulphotransferase activity	MF	1	0.028571429

GO:0033871	(heparan sulphate)-glucosamine-3-sulphotransferase-2-activity	MF	1	0.028571429
NS vs IPF				
GO:0009636	response to toxic substance	BP	2	0.142682927
GO:0097324	melanocyte migration	BP	1	0.073170732
GO:0097324	melanosome organization	BP	1	0.073170732
GO:0014031	mesenchymal cell development	BP	1	0.073170732
GO:0034204	lipid transport	BP	1	0.073170732
GO:0044429	mitochondrial part	CC	3	0.010787992
GO:0005739	mitochondrion	CC	5	0.034709193
GO:0030136	clathrin-coated vesicle	CC	1	0.073170732
GO:0000785	chromatin	CC	1	0.073170732
GO:0005766	primary lysosome	CC	1	0.073170732
GO:0000010	trans-hexaprenyltranstransferase activity	MF	1	0.073170732
GO:0050347	trans-octaprenyltranstransferase activity	MF	1	0.073170732
GO:0016887	ATPase activity	MF	1	0.073170732
GO:0070412	R-SMAD binding	MF	1	0.073170732

*p-value for genes that were significantly up- or downregulated.

here BP = biological process; CC= cellular component and MF= molecular function

Table 3: GO Enrichment Analysis of differentially expressed miRNAs in Lung tissue-derived exosomes

ID	Term	Ontology	n	p-value*
NS vs COPD				
GO:0048514	blood vessel morphogenesis	BP	12	0.068181818
GO:0050808	synapse organization	BP	11	0.0625
GO:0051962	positive regulation of nervous system development	BP	11	0.0625
GO:0044089	positive regulation of cellular component biogenesis	BP	10	0.056818182
GO:0044430	cytoskeletal part	CC	9	0.051136364
GO:0001525	angiogenesis	BP	8	0.045454545
GO:0050803	regulation of synapse structure or activity	BP	8	0.045454545
GO:0050807	regulation of synapse organization	BP	8	0.045454545
GO:0015630	microtubule cytoskeleton	CC	8	0.045454545
GO:0038023	signaling receptor activity	MF	8	0.045454545
GO:0060089	molecular transducer activity	MF	8	0.045454545
GO:0004888	transmembrane signaling receptor activity	MF	7	0.039772727
GO:0004930	G protein-coupled receptor activity	MF	7	0.039772727
GO:0019932	second messenger-mediated signaling	BP	6	0.034090909
GO:0007416	synapse assembly	BP	6	0.034090909

Preprints (www.preprints.org) | NOT PEER-REVIEWED | Posted: 27 August 2021 doi:10.20944/preprints202108.0520.v1

GO:0045765	regulation of angiogenesis	BP	5	0.028409091
GO:1901342	regulation of vasculature development	BP	5	0.028409091
GO:0051963	regulation of synapse assembly	BP	5	0.028409091
GO:0051965	positive regulation of synapse assembly	BP	4	0.022727273
GO:0019722	calcium-mediated signaling	BP	4	0.022727273
GO:0005815	microtubule organizing center	CC	4	0.022727273
GO:0005813	centrosome	CC	4	0.022727273
GO:0016525	negative regulation of angiogenesis	BP	3	0.017045455
GO:1901343	negative regulation of vasculature development	BP	3	0.017045455
GO:2000181	negative regulation of blood vessel morphogenesis	BP	3	0.017045455
GO:0033173	calcineurin-NFAT signaling cascade	BP	2	0.011363636
GO:0048016	inositol phosphate-mediated signaling	BP	2	0.011363636
GO:0097720	calcineurin-mediated signaling	BP	2	0.011363636
Sm Vs COPD				
GO:0048514	blood vessel morphogenesis	BP	11	0.071428571
GO:0044087	regulation of cellular component biogenesis	BP	11	0.071428571
GO:0044089	positive regulation of cellular component biogenesis	BP	10	0.064935065
GO:0051962	positive regulation of nervous system development	BP	10	0.064935065
GO:0001525	angiogenesis	BP	8	0.051948052
GO:0050803	regulation of synapse structure or activity	BP	8	0.051948052
GO:0050807	regulation of synapse organization	BP	8	0.051948052
GO:0044430	cytoskeletal part	CC	7	0.045454545
GO:0038023	signaling receptor activity	MF	7	0.045454545
GO:0060089	molecular transducer activity	MF	7	0.045454545
GO:0019932	second-messenger-mediated signaling	BP	6	0.038961039
GO:0007416	synapse assembly	BP	6	0.038961039
GO:0015630	microtubule cytoskeleton	CC	6	0.038961039
GO:0004888	transmembrane signaling receptor activity	MF	6	0.038961039
GO:0045765	regulation of angiogenesis	BP	5	0.032467532
GO:1901342	regulation of vasculature development	BP	5	0.032467532
GO:0051963	regulation of synapse assembly	BP	5	0.032467532
GO:0051965	positive regulation of synapse assembly	BP	4	0.025974026
GO:0019722	calcium-mediated signaling	BP	4	0.025974026
GO:0016525	negative regulation of angiogenesis	BP	3	0.019480519
GO:1901343	negative regulation of vasculature development	BP	3	0.019480519

GO:2000181	negative regulation of blood vessel morphogenesis	BP	3	0.019480519
GO:0005815	microtubule organizing center	CC	3	0.019480519
GO:0005813	centrosome	CC	3	0.019480519
GO:0004930	G-protein coupled recepor activity	MF	3	0.019480519
GO:0033173	calcineurin-NFAT signaling cascade	BP	2	0.012987013
GO:0048016	inositol phosphate-mediated signaling	BP	2	0.012987013
GO:0097720	calcineurin-mediated signaling	BP	2	0.012987013
NS Vs IPF				
GO:0065008	regulation of biological quality	BP	44	0.0327192
GO:0007399	nervous system development	BP	36	0.006858696
GO:0048878	chemical homeostasis	BP	18	0.003415
GO:0030030	cell projection organization	BP	17	0.012599483
GO:0120036	plasma membrane bounded cell projection organization	BP	17	0.01259943
GO:0044459	plasma membrane region	CC	10	0.028105097
GO:0007416	synapse assembly	BP	7	0.006212841
GO:0030424	axon	CC	7	0.0488352
GO:0150034	distal axon	CC	6	0.0305685
GO:0031349	positive regulation of defense response	BP	5	0.016747
GO:0044306	neuron projection terminus	CC	4	0.007341699
GO:0008092	cytoskeletal protein binding	MF	4	0.0073417
GO:0004930	G-protein coupled receptor activity	MF	4	0.083811139
GO:0051965	positive regulation of synapse assembly	BP	4	0.007341699
GO:0010863	positive regulation of phospholipase C activity	BP	2	0.01653348
GO:0043235	receptor complex	CC	2	0.01653348
GO:0023026	MHC class II protein complex binding	MF	2	0.0165335
GO:0005096	GTPase activator activity	MF	2	0.0165335
GO:1903997	positive regulation of non-membrane spanning protein tyrosine kinase activity	BP	2	0.01653348

*p-value for genes that were significantly up- or downregulated.

here BP = biological process; CC= cellular component and MF= molecular function

Table 4: KEGG Analyses of differentially expressed miRNAs in BALF-derived exosomes from COPD and IPF patients

KEGG pathway	Selected Pathway
COPD[ł]	
path:hsa00900	Terpenoid backbone biosynthesis
path:hsa04920	Adipocytokine signaling pathway

Preprints (www.preprints.org) | NOT PEER-REVIEWED | Posted: 27 August 2021 doi:10.20944/preprints202108.0520.v1

path:hsa00520	Amino sugar and nucleotide sugar metabolism
path:hsa04152	AMPK signaling pathway
path:hsa04371	Apelin signaling pathway
path:hsa04140	Autophagy-animal
path:hsa04136	Autophagy-other
path:hsa01040	Biosynthesis of unsaturated fatty acids
path:hsa04024	cAMP signaling pathway
path:hsa04218	Cellular senescence
path:hsa04062	Chemokine signaling pathway
path:hsa00534*	Glycosaminoglycan biosynthesis
IPF#	
path:hsa00900	Terpenoid backbone biosynthesis
path:hsa04920	Adipocytokine signaling pathway
path:hsa00520	Amino sugar and nucleotide sugar metabolism
path:hsa04371	Apelin signaling pathway
path:hsa04140	Autophagy-animal
path:hsa04136	Autophagy-other
path:hsa01040	Biosynthesis of unsaturated fatty acids
path:hsa04218	Cellular senescence
path:hsa04062	Chemokine signaling pathway
path: hsa05206	microRNAs in cancer

* significantly enriched pathway; ǂ COPD patients vs healthy controls (non-smokers and smokers); #IPF patients vs healthy non-smokers

Table 5: KEGG Analyses of differentially expressed miRNAs in lung tissue-derived exosomes from COPD and IPF patients

KEGG pathway	Selected Pathway
COPDǂ	
path:hsa04520	Adherens junction
path:hsa04920	Adipocytokine signaling pathway
path:hsa04261	Adrenergic signaling in cardiomyocytes
path:hsa04960	Aldosterone-regulated sodium reabsorption
path:hsa00520	Amino sugar and nucleotide sugar metabolism
path:hsa04215	Apoptosis-multiple species

Preprints (www.preprints.org) | NOT PEER-REVIEWED | Posted: 27 August 2021 doi:10.20944/preprints202108.0520.v1

path:hsa05310	Asthma
path:hsa05100	bacterial invasion of epithelial cells
path:hsa01040	Biosynthesis of unsaturated fatty acids
path:hsa04260	Cardiac muscle contraction
path:hsa04022	cGMP-PKG signaling pathway
IPF[#]	
path:hsa04972[*]	Pancreatic secretion
path:hsa04970[*]	Salivary secretion
path:hsa04911[*]	Insulin secretion
path:hsa05416[*]	Viral myocarditis
path:hsa05310	Asthma
path:hsa01040	Biosynthesis of unsaturated fatty acids
path:hsa04022	cGMP-PKG signaling pathway
path:hsa04014[*]	Ras signaling pathway
path:hsa04727[*]	GABAergic synapse
path:hsa05033[*]	Nicotine addiction
path:hsa04722[*]	Neurotrophin signaling pathway
path:hsa04010[*]	MAPK signaling pathway
path:hsa04151	PI3K-Akt signaling pathway

[*] significantly enriched pathway; [ł] COPD patients vs healthy controls (non-smokers and smokers); [#]IPF patients vs healthy non-smokers

Figure and Figure Legends

Preprints (www.preprints.org) | NOT PEER-REVIEWED | Posted: 27 August 2021 doi:10.20944/preprints202108.0520.v1

(i)

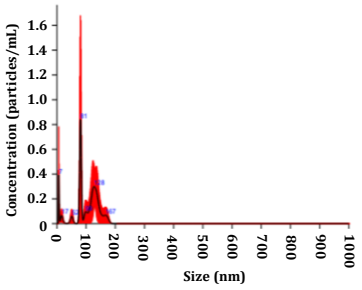

Conc (particle/mL) * 10^{10}	2.95 ± 2.2
Size (Mean,nm)	89.85 ± 28.4
Size (Mode, nm)	66.55 ± 22.4

(ii)

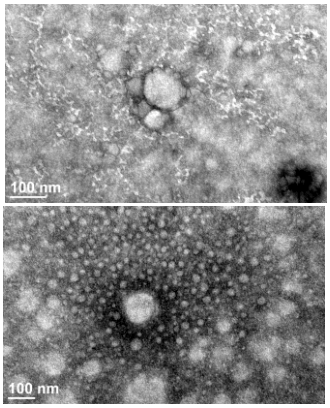

(iii)

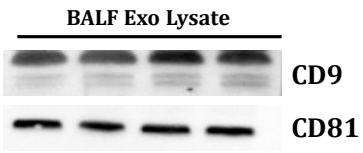

Figure 1: Characterization of human BALF-derived EVs/Exosomes. (i) Particle size depicted as mean, mode, and particle concentration were estimated using NanoSight NS300 (n=3-8/group). (ii) Representative TEM images of BALF-derived EVs/Exosomes (n=3). (iii) Immunoblot analysis of positive (CD9 and CD81) exosomal markers derived from human BALF (n=4).

Preprints (www.preprints.org) | NOT PEER-REVIEWED | Posted: 27 August 2021 doi:10.20944/preprints202108.0520.v1

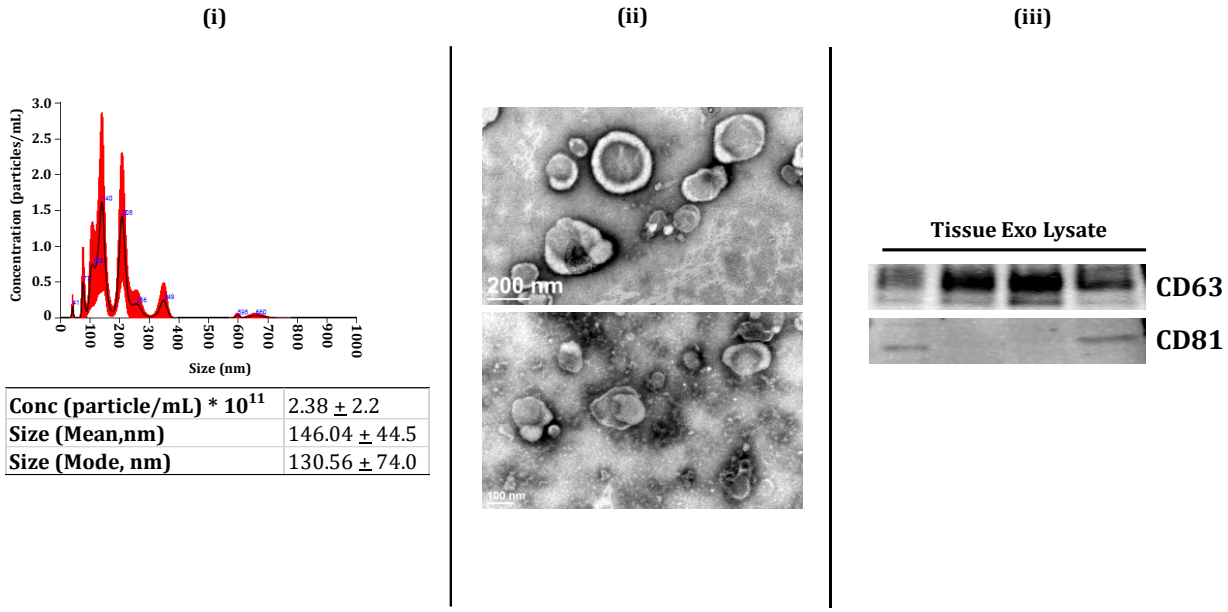

Conc (particle/mL) * 10^{11}	2.38 ± 2.2
Size (Mean,nm)	146.04 ± 44.5
Size (Mode, nm)	130.56 ± 74.0

Figure 2: Characterization of human lung tissue-derived EVs/Exosomes. (i) Particle size depicted as mean, mode, and particle concentration were estimated using NanoSight NS300 (n=3-5/group). (ii) Representative TEM images of lung tissue-derived EVs/Exosomes (n=6). (iii) Immunoblot analysis of positive (CD63 and CD81) exosomal markers derived from human lung tissue (n=4).

Preprints (www.preprints.org) | NOT PEER-REVIEWED | Posted: 27 August 2021 doi:10.20944/preprints202108.0520.v1

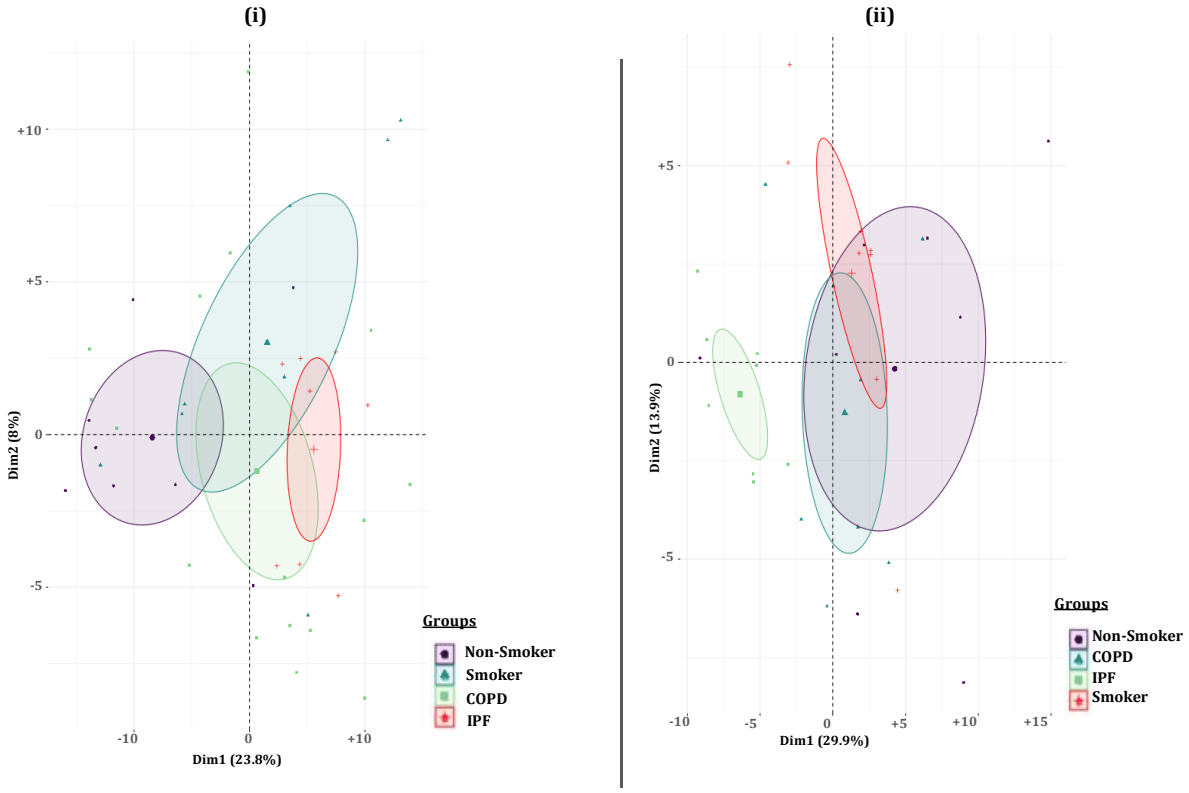

Figure 3: Principal Component Plot. Principal Component Analyses based on differential microRNA expression in individual (i) BALF- and (ii) Lung tissue-derived exosome samples from non-smokers, cigarette smokers, COPD and IPF subjects.

Preprints (www.preprints.org) | NOT PEER-REVIEWED | Posted: 27 August 2021 doi:10.20944/preprints202108.0520.v1

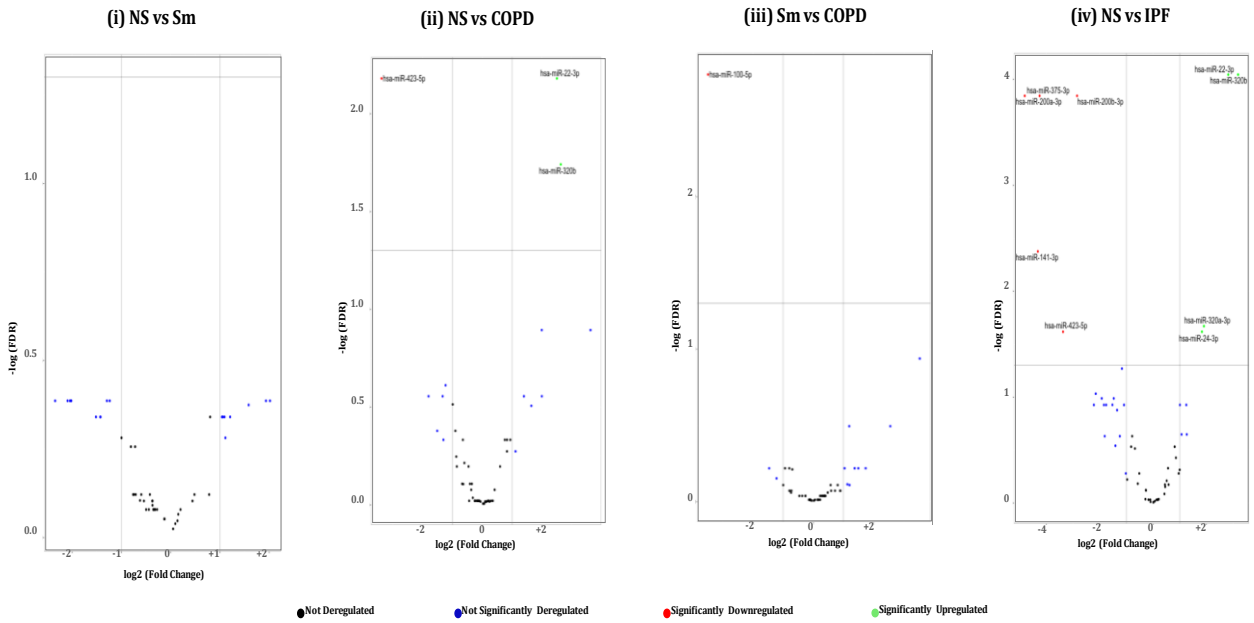

Figure 4: Volcano Plots showing number and distribution of miRNA from BALF-derived exosomes. Volcano plot showing the relation between –log(FDR) [Y-axis] vs log2(fold change) [X-axis] in the differentially expressed miRNAs amongst BALF exosomes derived from (i) healthy non-smokers (NS) vs healthy cigarette smokers (Sm), (ii) healthy non-smokers (NS) vs COPD patients (COPD), (iii) healthy cigarette smokers (Sm) vs COPD patients and (iv) healthy non-smokers (NS) and IPF patients (IPF).

Preprints (www.preprints.org) | NOT PEER-REVIEWED | Posted: 27 August 2021 doi:10.20944/preprints202108.0520.v1

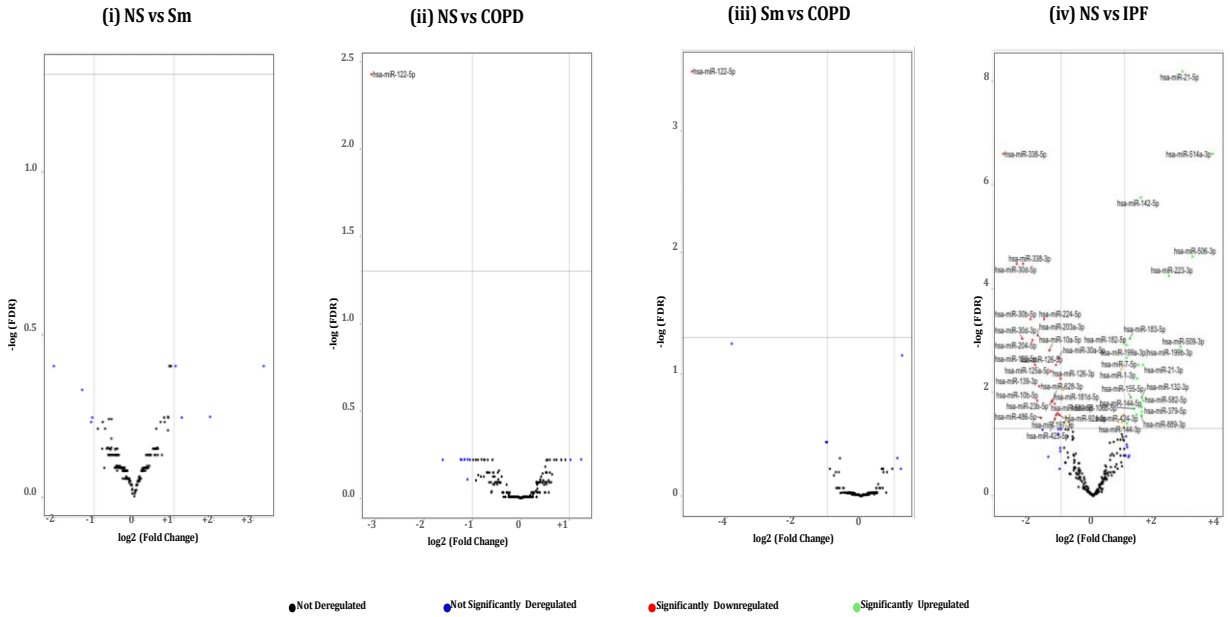

Figure 5: Volcano Plots showing number and distribution of miRNA from lung tissue-derived exosomes. Volcano plot showing the relation between –log(FDR) (Y-axis) vslog2(fold change) (X-axis) in the differentially expressed miRNAs amongst lung tissue exosomes derived from (i) healthy non-smokers (NS) vs healthy cigarette smokers (Sm), (ii) healthy non-smokers (NS) vs COPD patients (COPD), (iii) healthy cigarette smokers (Sm) vs COPD patients and (iv) healthy non-smokers (NS) and IPF patients (IPF).

Preprints (www.preprints.org) | NOT PEER-REVIEWED | Posted: 27 August 2021 doi:10.20944/preprints202108.0520.v1

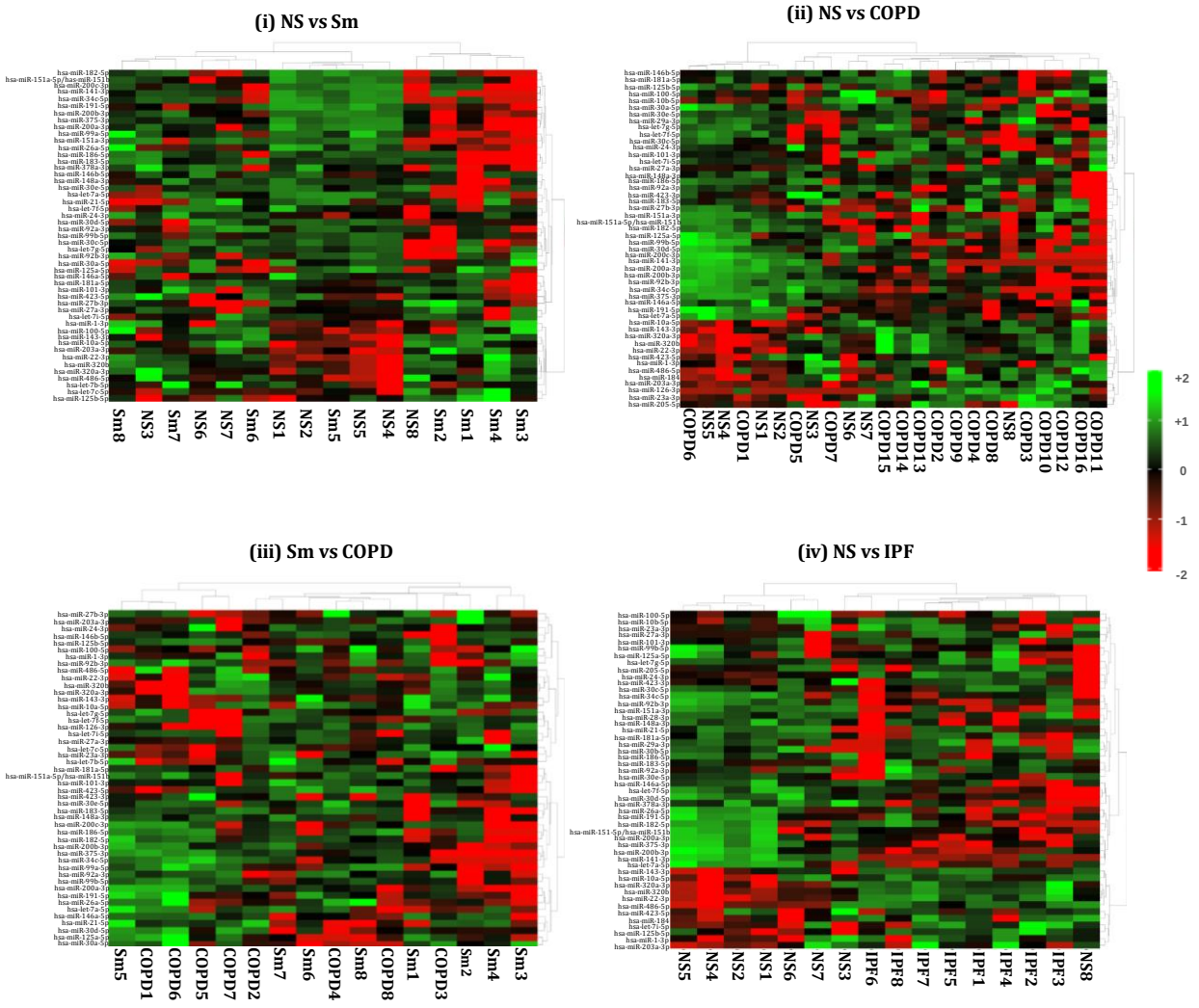

Figure 6: Hierarchical cluster analyses of differentially expressed miRNAs from BALF-derived exosomes. Heat map showing top 50 variable miRNAs that are differentially expressed in the BALF-derived exosomes from (i) healthy non-smokers (NS) vs healthy smokers (Sm), (ii) healthy non-smokers (NS) vs COPD patients (COPD), (iii) healthy smokers (Sm) and COPD patients (COPD) and (iv) healthy non-smokers (NS) and IPF patients (IPF).

Preprints (www.preprints.org) | NOT PEER-REVIEWED | Posted: 27 August 2021 doi:10.20944/preprints202108.0520.v1

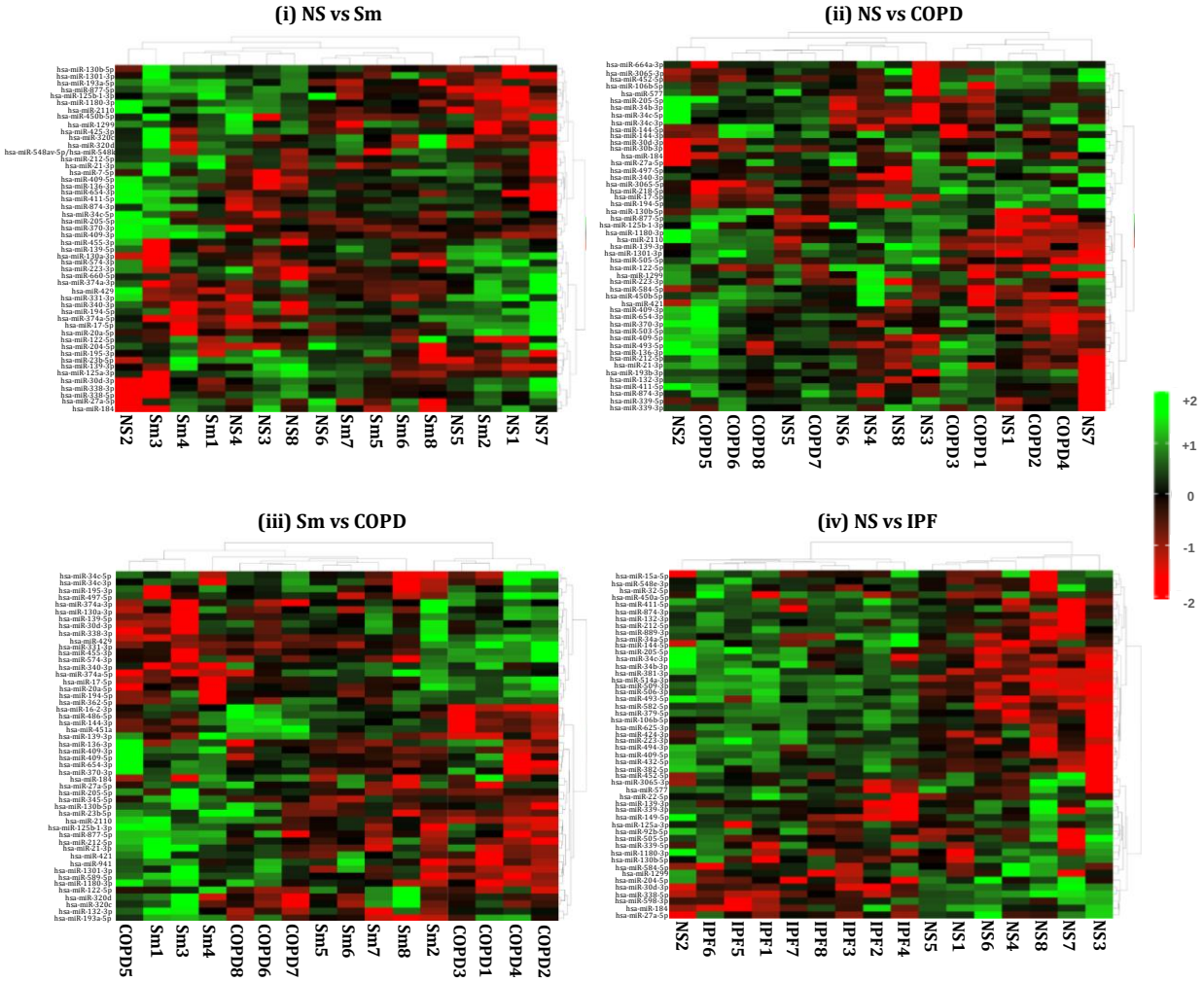

Figure 7: Hierarchical cluster analyses of differentially expressed miRNAs from lung tissue-derived exosomes. Heat map showing top 50 variable miRNAs that are differentially expressed in the lung tissue-derived exosomes from (i) healthy non-smokers (NS) vs healthy smokers (Sm), (ii) healthy non-smokers (NS) vs COPD patients (COPD), (iii) healthy smokers (Sm) and COPD patients (COPD) and (iv) healthy non-smokers (NS) and IPF patients (IPF).

Supplementary Tables

Supplementary Table 1: Significant Differentially expressed miRNAs in BALF derived exosomes.

Preprints (www.preprints.org) | NOT PEER-REVIEWED | Posted: 27 August 2021 doi:10.20944/preprints202108.0520.v1

miRNA	log2foldchange	logCPM	pvalue	FDR	Functional Annotation
NS vs COPD					
hsa-miR-423-5p	-3.389204282	14.75498	0.00013369	0.0066	mRNA binding involved in posttranscriptional gene silencing. Role in apoptosis and cell proliferation
hsa-miR-320b	2.638473041	14.15853	0.00098978	0.01815	tumor suppressing role by targeting CDK6
hsa-miR-22-3p	2.508785494	18.34373	0.00023988	0.0066	negative regulator of endothelial cell proliferation and necroptotic process; but positive regulator of inflammatory response
Sm vs COPD					
hsa-miR-100-5p	-3.492285687	18.86802	3.29E-05	0.00158	negative regulation of cell differentiation and IL-8 secretion
NS vs IPF					
hsa-miR-200a-3p	-4.811568605	13.79069	7.88E-06	0.00014	positive regulator of blood vessel endothelial migration, role in Endothelial-mesenchymal transition
hsa-miR-141-3p	-4.31928888	11.4448	0.00045173	0.00422	positive regulator of cell proliferation and negative regulator of leukocyte adhesion to vascular endothelial cell
hsa-miR-375-3p	-4.255714743	12.47332	1.28E-05	0.00014	RNA polymerase II binding complex; positive regulator of endothelial cell apoptotic process
hsa-miR-423-5p	-3.37545635	14.95874	0.00376795	0.02416	mRNA binding involved in posttranscriptional gene silencing. Role in apoptosis and cell proliferation
hsa-miR-320b	3.186119102	14.24854	3.22E-06	9.03E-05	tumor suppressing role by targeting CDK6
hsa-miR-200b-3p	-2.849476778	14.33963	1.21E-05	0.00014	positive regulator of cell proliferation; negative

Preprints (www.preprints.org) | NOT PEER-REVIEWED | Posted: 27 August 2021 doi:10.20944/preprints202108.0520.v1

					regulator of gene expression
hsa-miR-22-3p	2.817552446	18.23789	3.10E-06	9.03E-05	negative regulator of endothelial cell proliferation and necroptotic process; but positive regulator of inflammatory response
hsa-miR-320a-3p	1.906370214	14.44337	0.0026728 2	0.0213 8	negative regulator of cell proliferation, cell migration and IL-4 biosynthetic process.
hsa-miR-24-3p	1.83111351	12.04935	0.0038836 4	0.0241 6	negative regulator of angiogenesis and blood vessel endothelial cell migration

Supplementary Table 2: Significant Differentially expressed miRNAs in Lung-derived exosomes.

miRNA	log2foldchange	logCPM	pvalue	FDR	Function
NS vs COPD					
hsa-miR-122-5p	-3.081717764	8.0592	1.66E-05	0.0037 4	cell proliferation, migration, invasion, and EMT
Sm vs COPD					
hsa-miR-122-5p	-5.048802634	9.96494	1.64E-06	0.0003 3	cell proliferation, migration, invasion, and EMT
NS vs IPF					
hsa-miR-514a-3p	3.779748499	4.04505	3.15E-09	2.56E-07	Tumor suppressor
hsa-miR-506-3p	3.146428357	5.6144	4.98E-07	2.43E-05	negative regulator of cellular biosynthetic pathwaya and IL8 secretion
hsa-miR-21-5p	2.828829977	15.6156	2.70E-11	6.58E-09	negative modulator of angiogenesis; regulates extracellular matrix degradation

Preprints (www.preprints.org) | NOT PEER-REVIEWED | Posted: 27 August 2021 doi:10.20944/preprints202108.0520.v1

hsa-miR-338-5p	-2.821754174	8.55174	2.59E-09	2.56E-07	negative regulation of IL6 secretion and cell migration
hsa-miR-509-3p	2.767633188	5.4511	8.72E-05	0.00133	negative regulator of cell migration, invasion and proliferation
hsa-miR-223-3p	2.402273957	8.20475	1.88E-06	5.74E-05	negative regulator of GTPase activity and regulated macrophage differentiation
hsa-miR-30d-5p	-2.400812469	16.3117	8.89E-07	3.35E-05	regulates gene expression and EMT
hsa-miR-30d-3p	-2.22958366	5.29936	4.73E-05	0.00094	inhibitor of cell proliferation and invasion
hsa-miR-338-3p	-2.204598086	7.29224	9.62E-07	3.35E-05	negative regulator of cell migration and IL6 production
hsa-miR-30b-5p	-1.967255645	12.7584	1.59E-05	0.00039	positive regulator of TGF-beta signaling pathway, regulates lipid metabolism, association with senescence
hsa-miR-204-5p	-1.904426753	5.64924	5.69E-05	0.00099	negative regulation of IL6, IL1beta production and cell migration, regulates EMT
hsa-miR-122-5p	-1.822688383	8.34723	0.00025	0.00299	cell proliferation, migration, invasion, and EMT
hsa-miR-10b-5p	-1.754493357	13.4712	0.00202	0.01452	positive regulator of cell migration, Th17 regulator
hsa-miR-203a-3p	-1.740223733	10.5438	3.65E-05	0.00081	negative regulator of IL8 secretion, regulates EMT
hsa-miR-139-3p	-1.692253283	4.65751	0.00088	0.0077	Tumor suppressor, EMT
hsa-miR-486-5p	-1.636372182	13.0762	0.00604	0.03137	regulates gene expression and has been shown to be associated with IPF
hsa-miR-582-5p	1.590929655	3.94706	0.00196	0.01452	tumor suppressor
hsa-miR-21-3p	1.582268505	7.57847	0.00027	0.00299	negative modulator of angiogenesis; regulates extracellular matrix degradation
hsa-miR-379-5p	1.553371104	4.88324	0.00385	0.02409	negative regulator of cell proliferation and positive regulator of apoptosis
hsa-miR-132-3p	1.543109071	5.19083	0.00161	0.0128	negative regulator of gene expression, regulates

Preprints (www.preprints.org) | NOT PEER-REVIEWED | Posted: 27 August 2021 doi:10.20944/preprints202108.0520.v1

					inflammation and cell proliferation
hsa-miR-224-5p	-1.541206326	9.28135	1.55E-05	0.00039	regulates cell proliferation, migration and invasion through PIK3R3/Akt pathway
hsa-miR-144-5p	1.53599799	5.70304	0.00293	0.01932	negative regulator of EMT; positive regulation of mitochondrial organization
hsa-miR-889-3p	1.534772448	4.45827	0.00534	0.02833	regulates cell viability and invasion
hsa-miR-142-5p	1.514303487	8.17025	2.93E-08	1.79E-06	negative regulation of IL1beta, response to TNF
hsa-miR-7-5p	1.436816898	5.84014	0.00027	0.00299	inhibits cell migration and invasion, suppresses tumor metastasis
hsa-miR-1-3p	1.398003997	9.02882	0.00059	0.00551	cell proliferation and invasion
hsa-miR-424-3p	1.377444275	3.95708	0.00457	0.02718	negative regulation of cell proliferation and invasion, negative regulation of fibroblast growth factor receptor signaling
hsa-miR-10a-5p	-1.373153961	15.8906	0.00011	0.00157	cell migration and endothelial growth factor signaling
hsa-miR-125a-5p	-1.318243293	14.1273	0.00041	0.00397	fibroblast transdifferentiation, negative regulation of IL16
hsa-miR-106b-5p	1.308396822	4.51807	0.00325	0.02087	regulates EMT and TGF beta signaling, negative regulator of IL8
hsa-miR-23b-5p	-1.300249004	5.24808	0.00219	0.01524	TGF beta signaling regulation
hsa-miR-628-3p	-1.275911117	6.31838	0.00199	0.01452	regulator of cell proliferator
hsa-miR-181d-5p	-1.204679475	6.05627	0.00246	0.01669	inhibitor of cell proliferation and metastasis
hsa-miR-155-5p	1.199631772	7.4596	0.00163	0.0128	negative regulator of cytokine secretion and regulates epithelial barrier and EMT
hsa-miR-197-3p	-1.197907775	5.53844	0.00663	0.03303	negative regulation of IL-18
hsa-miR-183-5p	1.168387995	11.1446	4.99E-05	0.00094	TGF-beta signaling, positive regulation of phagocytosis
hsa-miR-126-5p	-1.161697617	10.4425	0.00028	0.00299	negative regulator of cell migration

Preprints (www.preprints.org) | NOT PEER-REVIEWED | Posted: 27 August 2021 doi:10.20944/preprints202108.0520.v1

hsa-miR-423-5p	-1.158386165	11.3123	0.00472	0.02741	negative regulator of cell invasion and migration
hsa-miR-589-5p	-1.113954446	5.58091	0.00416	0.0254	regulates EMT
hsa-miR-30a-5p	-1.077861429	14.4068	0.00017	0.00219	regulator of TGF-beta signaling
hsa-miR-144-3p	1.07056553	7.30821	0.00874	0.04023	negative regulator of EMT and positive regulator of mitochondrial organization
hsa-miR-199a-3p|hsa-miR-199b-3p	1.068687434	12.3784	0.00017	0.00219	positive regulator of endothelial cell migration, negative regulation of autophagy
hsa-miR-182-5p	1.0640442	11.2871	7.58E-05	0.00123	positive regulator of cell migration and cytokine secretion
hsa-miR-92a-3p	-1.061586028	11.5755	0.00486	0.02742	regulates TGF-beta signalling
hsa-miR-126-3p	-1.020449014	12.1275	0.00061	0.00551	role in angiogenesis and vascular homeostasis
hsa-miR-340-5p	0.968709958	7.35372	0.00494	0.02742	regulates cell proliferation
hsa-miR-409-3p	0.957771401	6.15189	0.01087	0.04821	promotes tumorigenesis
hsa-miR-30a-3p	-0.932099425	10.06	0.00107	0.00904	negative regulator of EMT
hsa-miR-146b-5p	0.920971946	15.3479	0.00797	0.03815	negative regulator of endothelial activation, EMT and IL17 pathway
hsa-miR-148a-3p	0.903657387	12.9195	0.00036	0.00362	role in tumor suppression
hsa-miR-342-3p	-0.890916332	9.21854	0.00834	0.03915	regulates TGF-beta signaling
hsa-miR-151b	-0.840780828	7.66417	0.0062	0.03153	represses cell migration
hsa-miR-103a-3p	0.80597023	9.14838	0.00769	0.03754	negative regulation of peptidyl-threonine phosphorylation, regulates glucose homeostasis
hsa-miR-186-5p	-0.734165882	11.605	0.00512	0.02778	regulates collagen and EMT
hsa-miR-151a-5p|hsa-miR-151b	-0.72411126	12.6144	0.00951	0.04297	regulates cell proliferation, migration and invasion